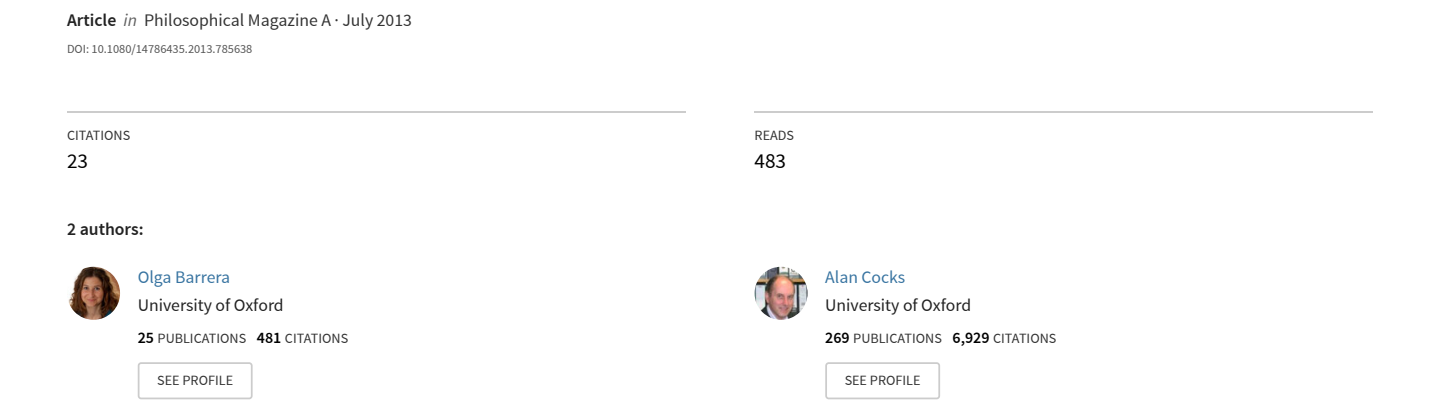
# Computational modelling of hydrogen embrittlement in welded structures



Magazine Computa-

Philosophical Magazine
Vol. 00, No. 00, 00 Month 2010, 1–17

#### RESEARCH ARTICLE

# Computational modelling of hydrogen embrittlement in welded structures

O. Barrera<sup>a</sup> \* and A.C.F. Cocks<sup>a</sup>

<sup>a</sup> Engineering Science Department, University of Oxford, Parks Road, OX1 3PJ, UK; (Received 00 Month 200x; final version received 00 Month 200x)

This paper deals with the modelling of the combined hydrogen embrittlement phenomena: hydrogen enhanced local plasticity (HELP) and hydrogen induced decohesion (HID) in dissimilar welds through a cohesive zone modelling approach (CZM). Fractured samples of dissimilar weld interfaces in AISI8630/IN625 show that cracks propagate in a region called the "featureless" region located in the Nickel side of the weld. This region is characterized by the presence of a distribution of fine  $M_7C_3$  carbides. We model the effect of hydrogen on the material toughness as the result of a synergistic effect of HELP and HID mechanisms where (i) hydrogen enhanced dislocation mobility promotes the development of dislocation structures at the  $M_7C_3$  carbides which increases the stress on the particles; while the presence of hydrogen also results in (ii) a reduction in the (a) cohesive strength of the carbide/matrix interface and (b) in the local flow stress of the matrix. The decohesion mechanism at the carbide/matrix interface is modelled through a two dimensional user-defined cohesive element implemented in a FORTRAN subroutine (UEL) in the commercial finite element code ABAQUS and the effect of the hydrogen on the plasticity properties of the matrix is coded in a UMAT routine. Preliminary analysis on a unit cell representing the matrix/carbide system under plane strain shows that HELP and HID are competitive mechanisms. When the combined mechanism HELP+HID occurs micro-cracks form at the matrix/carbide interface due to decohesion process followed by localization of plastic flow responsible for the link-up of the micro-cracks.

Keywords: dissimilar welds; hydrogen embrittlement; cohesive zone modelling.

#### 1. Introduction

It is well know that hydrogen reduces the service life of many welded components by causing mechanical degradation of all metallic systems, often resulting in failure of structural components far below their design limits, see for example [1-12]. Hydrogen cracking is the most significant, yet least understood, mechanism of failure experienced by engineering components. The presence of hydrogen, either as an external gas, resulting from electrochemical reactions in a marine environment or dissolved in the molten metal during processing, clearly leads to a severe degradation in the material properties and consequently a loss in structural integrity of a vast range of metals and alloys. In particular, high strength ferritic steels used for pipelines, pressure vessels and compressors are prone to hydrogen cracking [2,13]. A unique fracture mode characteristic of hydrogen cracking does not exist, as this phenomenon is a synergistic effect of mechanisms due to electrochemical reactions, metallurgy, hydrogen diffusion, solubility processes and loading conditions. Hydrogen assisted cracking fracture morphologies and failure processes depend on a vast

 $<sup>{\</sup>rm *Corresponding\ author.\ Email:\ olga.barrera@eng.ox.ac.uk}$ 

O. Barrera and A.C.F. Cocks

number of variables: material system, temperature, environmental pressure, grain boundary impurity composition, loading rate, stress intensity factor level, yield strength, boundary conditions, etc...

The different failure mechanisms of hydrogen cracking have been classified into five categories [6]: cracking from hydride formation; hydrogen induced blistering; hydrogen attack; cracking due to precipitation of internal hydrogen and hydrogen embrittlement. The most severe phenomenon seen in ferritic steels and dissimilar welds has been recognized to be hydrogen embrittlement. Hydrogen embrittlement has received significant attention in the scientific and engineering literature due to its impact on the structural integrity of components in the oil and gas industries. The micromechanical processes associated with hydrogen embrittlement can be grouped into three categories: i. HELP: hydrogen enhanced localized plasticity, ii. HID: hydrogen induced decohesion, iii. HIPT: hydrogen induced phase transformation [16] although a combination of more than one mechanism (HELP and HID) is, at the present time, one of the most widely accepted mechanisms [14–17]. Dissimilar metal butter-welded joints are commonly used by the oil and gas industries to join a range of structural components such as valves, connectors, manifolds to carbon steel pipes, as they allow a welded connection between high strength hardenable carbon forged steel or non-hardenable pipe line steel to Nickel alloy components [10, 16, 31, 33]. A series of catastrophic failures of AISI 8630 steel/IN625 Nickel alloy dissimilar-metal welds which occurred in the North Sea and in the Gulf of Mexico [16] highlighted the need for further investigations on the role of the hydrogen on the fracture process of the components. The focus of this paper is on computational modelling of hydrogen embrittlement in AISI8630/IN625 dissimilar welds.

One of the outstanding issues in hydrogen cracking of welds is to link micromechanical processes to the macroscopic fracture behaviour of the system. Recent TEM and SEM studies [10, 16, 31, 33] have revealed detailed information about the microstructure in the vicinity of the fusion boundary of 8630/625 dissimilar welds and the fracture morphologies which alternates between a flat cleavage-like morphology and a highly irregular cratered structure. In this paper we use these experimental observations to guide the development of a model of the combined hydrogen embrittlement phenomena (HELP + HID).

Central to the development of the model is the use of a cohesive zone modelling approach (CZM). In the last decade CZM has gained interest in the field of fracture modelling. CZM is widely used to represent the fracture process at different scales. The basic idea of modelling deformation and finally the decohesion of the material at a crack tip or at the interface between two dissimilar materials by a traction separation law was given by Barenblatt [21] and Dugdale [22] and further developed by [21-26]. Cohesive elements can be imagined as interface elements with a thickness close to zero embedded in continuum elements. Fracture occurs at the interface between the CZM and continuum elements. One of the key properties of a CZM is the definition of the traction-separation  $(T-\delta)$  law. In this paper a cohesive element formulation is proposed in which the T- $\delta$  law is a function of hydrogen content and the plastic deformation of the surrounding material. This model has been implemented as a user element (UEL) in the commercial finite element code ABAQUS. Following Sofronis et al. [14] we also assume that the constitutive response of the material is also a function of the hydrogen content. An appropriate model is identified and this has been implemented in a UMAT ABAQUS routine. The organization of the paper is as follows. Section 2 presents a summary of the hydrogen cracking mechanism with a focus on hydrogen embrittlement by a combined HELP and HID mechanism. In Section 3 an overview of the microstructure

Philosophical Magazine

and fracture surface morphology of dissimilar welds is given. In Section 4 the model of the combined HELP and HID mechanisms is presented. Section 5 shows a number of numerical simulations where we explore the interaction between interface decohesion and matrix plastic deformation.

#### 2. Hydrogen cracking mechanisms

Structures subjected to concurrent mechanical loading and hydrogen gas exposure become more susceptible to cracking due to the ability of hydrogen molecules to dissociate into hydrogen atoms on metal surfaces, which then diffuse into the metal. Hydrogen cracking has been explained through several mechanisms: (i) cracking from hydride formation, (ii) hydrogen induced blistering, (iii) hydrogen attack, (iv) cracking due to precipitation of internal hydrogen, (v) hydrogen embrittlement (AMS Materials Handbook [6]). Although the focus of the paper is hydrogen embrittlement (HE), the mechanisms (i), (ii), (iii), (iv) present some features that are also experienced by HE and it is instructive to review these here. Cracking from hydride formation occurs where highly brittle hydride precipitates form resulting in a "low energy" fracture path. Zirconium, titanium, tantalum and other transition metals form hydrides when the hydrogen content exceeds the solubility limit. These hydrides are brittle compounds characterized by low density, and produce degradation of the ductility of the alloy. Hydride formation and cleavage fracture occur in systems where hydrides are stable or can be stabilized by application of stress. Microscopical observations and thermodynamic analysis confirm this process [28–30]. Comparisons between phase diagrams of hydride-forming systems and non hydride-forming systems explain the intrinsic difference in the hydrogen damage processes. The maximum solubility of hydrogen in Ti-H, Vb-H and Zr-H is higher than in Fe-H or Ni-H, Al-H and other metal-H systems. Exceeding the hydrogen solubility limit in Al or Fe results in hydrogen gas bubbles precipitating in the material lattice leading to hydrogen blistering or other cracking mechanisms. The focus of the present work is the Fe/Ni dissimilar welds hence the paper is primarily concerned with cracking in non-hydride forming systems.

Hydrogen blistering occurs when hydrogen atoms collect at extraordinary sites (including the interface between inclusions and metallic matrix) and recombine to generate a pressure at the interfaces. Factors that influence the magnitude of the hydrogen gas pressure are: (i) the hydrogen concentration, (ii) the ratio between the trapped hydrogen and the hydrogen in the lattice and (iii) the temperature. When the hydrogen is absorbed due to electrochemical reactions or cathodic protection the interface pressure can become significant. Bumps or blisters will form at the interfaces where the concentration of hydrogen reaches a certain level, which form as the result of local plastic deformation under the internal pressure that is generated locally. In addition, the hydrogen may alter the deformation mechanism and the fracture morphology of the metal. At the tips of blisters high tensile triaxial stress states are generated which provides favourable sites for hydrogen to accumulate. Blisters will continue to grow as the concentration of hydrogen increases. The ductility of the metal reduces as the hydrogen content increases. This decrease in ductility becomes more significant in high strength alloys. So high strength steels are prone to this type of fracture.

**Hydrogen attack** is related to the interaction between hydrogen and alloying elements in the microstructure that form a gaseous phase. Metal components subjected to high temperature and high pressure experience microstructural change and degradation in strength leading to fracture. Decarburisation is the

intergranular fracture morphology.

Computa-

reaction between hydrogen in the environment and carbon in steel. The product of the reaction is methane that is then released in the surrounding environment. Decarburization produces a decrease of the carbon content in the area where the carbides begin to dissociate. Methane is not soluble in steel hence it remains trapped in defects and micro pores. The methane pressure in the pores might become significant to allow the pores to grow. The combination of the gas pressure and the applied stress may lead to a creep-like growth process of the pores. The pores can then coalesce to form microcracks which in turn link, leading to failure.

Pores often form and grow preferentially on grain boundaries, giving rise to an

O. Barrera and A.C.F. Cocks

Cracking from precipitation of internal hydrogen occurs during forging, casting and welding when the hydrogen is absorbed in the molten metal. During solidification the excess hydrogen precipitates at voids, defects and interfaces. The pressure increases in the locations where hydrogen precipitates creating an increase of the stress level at these defects, leading to a macroscopic brittle failure. The cracks resulting from this process are called "fish eyes" (in service) or "flakes" (during processing) and they form a macroscopic brittle intergranulal type of fracture.

The discussion of these hydrogen cracking mechanisms give some insight into the effect of hydrogen on metals and alloys. The most important phenomenon, however, observed in high strength steel and dissimilar welds is hydrogen embrittlement. This mechanism is the focus of this paper and it is discussed in the following subsection.

### 2.1. Hydrogen embrittlement: HELP and HID

Hydrogen embrittlement (HE) may occur after the component has been in service for many years. The meaning of the term "embrittlement" has been referred to an overall reduction of ductility and a fracture surface that is generally macroscopically intergranular. HE is responsible for a sharp transition from a high-toughness ductile fracture (microvoid coalescence) to a brittle-type of fracture, leading to a significant reduction of strength and ductility. There is no single mechanism that causes hydrogen-induced failure. The effect of hydrogen on the reduction of an overall ductility can be summarized into two main phenomena: HELP (Hydrogen enhanced local plasticity) and HID (hydrogen induced decohesion). Evidence supporting the **HELP** mechanism is well documented, see [3, 9], [13-18] amongst others. Experimental observations and accurate fractography show that hydrogen in solid solution enhances the dislocation mobility by lowering the barriers to dislocation motion, consequently causing softening of the material, strain localization and fracture. Failure is due to highly localized plasticity which limits the macroscopic ductility, rather than an embrittlement process. This phenomenon has been observed in fcc, bcc and hcp systems of pure materials, solid solution alloys and precipitation strengthened alloys. TEM and SEM studies of the microstructure from site-specific locations reveal a quasi cleavage fracture surface where the surface has ridges (Fig.3) that can be correlated with sub-surface intense and highly localized deformation bands [13, 20].

Hydrogen induced decohesion (**HID**) is one the earliest theories for HE proposed in the literature [33-36]. The hypothesis which underpins the decohesion model is that dissolved hydrogen atoms in the lattice, grain boundary or interfaces lower the force required to separate the crystal along a crystallographic plane, grain boundary or particle/matrix interface. Hydrogen reduces the cohesive force as well

as the corresponding energy to form a cleavage surface. The decohesion theory postulates that cracking occurs when a local tensile stress is sufficiently high to equal the maximum local cohesive stress. There are some observations that support this theory in non-hydride forming systems such as: (i) the appearance of the fracture surfaces, (ii) ab-initio calculations of the effect of the hydrogen on grain boundary cohesion in Nickel and on the fracture energy of Fe and Al [2]. The HID mechanism is not universally accepted due to the lack of direct experimental observations and the inability to measure the cohesive forces. Moreover, the lack of knowledge on the cohesive strength law as a function of local hydrogen

Recent theories of HE investigate the effect of hydrogen on the material toughness due to a synergistic action of HELP and HID [15, 17]. Based on experimental evidence of HE in quenched and tempered martensitic high-strength steels, Novak et al. [17] proposed a model of hydrogen-induced intergranular failure where failure is initiated by decohesion at grain-boundary carbide particles due to dislocations piling-up at the matrix-carbide interface. The effect of hydrogen on dislocation mobility enhances the formation of a dislocation pile-up on a grain boundary carbide, leading to decohesion at carbide/matrix interfaces and in turn intergranular fracture. This type of mechanism has also been observed in Nickel-based welds [16]. A description of the dissimilar-metal welds microstructure AISI8630/IN625 is given in the following section.

concentration is one of the outstanding issues reported in the literature.

## ${\bf 3.} \quad {\bf Dissimilar-metal\ welds\ microstructure:\ AISI8630/IN625}$

Nickel-based welds are largely used by the oil and gas industry to facilitate the welding of the high strength steel pipes to other alloy forgings. A nickel-based butter layer is deposited on top of the high strength steel, which is then welded to the alloy forging. In order to prevent corrosion of the piping system subsea cathodic protection is applied. Although cathodic protection prevents corrosion, one of the potential effects is the absorption of hydrogen into the metal lattice. It can also concentrate in plastically deformed areas as well as in extraordinary sites (grain boundaries, inclusions, precipitate, dislocation etc...). Figure 1 [50] shows a simplification of the interface microstructure of a 8630/625 dissimilar weld [31, 32], i.e. at the interface between the steel and the buttering. Three major regions can be distinguished:

- a. The heat affected zone (HAZ) in the parent steel side close to the interface consists of a fine decarburised zone. This zone is mostly ferritic.
- b. A martensitic iron rich region (about  $1\mu m$  wide) on the steel side close to the fusion boundary. This zone exhibits a BCT structure.
- c. A FCC region (about  $20\mu m$  wide) in the nickel side previously wrongly identified as a "featureless zone" that plays an important role in the macroscopic fracture behaviour of the system in a hydrogen environment [50]. A fine distribution of high atomic number  $M_7C_3$  carbides has recently been observed in this zone [13, 20, 50]. The volume fraction has been estimated to be about 20% and the dimension of the major axis of the carbides is about 40nm.

#### 3.1. HELP and HID in dissimilar welds AISI8630/IN625

Figure 2 [51] shows a fractured sample of an AISI8630/IN625 dissimilar weld exposed to a hydrogen rich environment. The crack path with respect to the interface

Computa-

structure of figure 2 is shown in figure 3, which has sections within (a) the HAZ, (b) the martensitic region and (c) the featureless zone. Despite the crack initiation

location not being precisely identified [16, 31, 32] and is still subject to debate, there is general agreement that the presence of  $M_7C_3$  carbides in the "featureless"

zone" provides a low energy path for crack propagation.

The fracture morphology of this region consists of terrace-cleavage or quasi cleavage features (Fig.2). More in-depth studies of this type of fracture in pipeline steels [13, 20] has revealed that the planes along which the cracks propagate are not known cleavage planes. The planes contain ridges that are almost parallel to the crack propagation path. These ridges are related to sub-surface intense and highly localized deformation bands [13]. The fracture surface appears to be generated by ductile processes, enhanced and localized to well defined slip bands by hydrogen [20]. Although the fcc structure of the featureless region of a dissimilar weld is different to that of steels, the fracture morphology is characteristic of this cleavage-like or terraced type of fracture (Fig. 2). Ridges characteristic of the intense localised plastic deformation process are evident on the quasi cleavage faces shown in the higher magnification micrograph of Fig. 4.

An higher magnification image of the "crater" region (Fig. 4) demonstrates that the shape of these "dimples" (of the order of 100nm) are consistent with the size of martensitic lath bundles, with banded features on these craters consistent with the characteristic width of the laths. Hence the crater area is essentially a martensitic region as labelled in Fig. 3. The third region of the failure surface is through the HAZ and is again characteristic of a local cleavage process.

The relative proportions of the three different regions on the failure surface depends on the hydrogen concentration. The area fraction associated with the featureless zone increases with increasing hydrogen content and dominates at high hydrogen concentrations [51]. We therefore concentrate on the failure process within this zone in the remainder of this paper.

The fracture morphology within the featureless zone, which is produced only in the presence of hydrogen, is consistent with a hydrogen-induced decohesion (HID) mechanism along the  $M_7C_3$ -matrix interface succeeded by strain localization between the particles. This suggests that the effect of hydrogen on the material toughness is a result of a synergistic effect of HELP and HID mechanisms: (i) with hydrogen enhancing dislocation mobility, promoting softening and strain localization; (ii) and the combined effect of increased stress on the  $M_7C_3$  carbides due to the enhanced plastic deformation and the effect of hydrogen on the interface cohesive properties promoting decohesion at the particle/matrix interface. These observations suggest that cracks nucleate at the interface of the  $M_7C_3$  particles in the featureless zone under the high stresses generated locally. These interfacial cracks link with each other and the main crack through localised, intense, plastic deformation. In this paper we use: (i) classical models of the plastic deformation of particle strengthened materials to evaluate the short range interaction between dislocation loops and particles, which is not captured by purely continuum models, and (ii) a cohesive zone modelling approach to model the decohesion process at the carbide/matrix interface.

#### 4. Modelling decohesion at the metal carbide interface

Here we are interested in modelling crack nucleation and growth at the interface of  $M_7C_3$  carbides particles that are distributed throughout the matrix (in the featureless zone). Models of the nucleation of cavities at particles fall into two major categories; either the energy released reaches a critical value or a critical stress is

reached at the particle/matrix interface, as described by Goods and Brown [42] and Garrison and Moody [43]. The energy criterion provides a necessary but not sufficient condition for nucleation, while the critical stress approach provides a mechanism of nucleation. In practice, it is generally agreed that both these conditions need to be satisfied. For particles larger than about 500A the energy condition is met at small plastic strains [42, 43, 48] and nucleation is determined by achieving a critical stress at the interface while at smaller particles the energy criterion is the controlling factor. Cohesive zone models inherently provide a mechanism for decohesion at an interface, while at the same time satisfying the requirement that enough energy is available to form a crack. Thus, if suitably calibrated they naturally satisfy both the mechanistic and energy requirements. Novak et al. [17] adapted the dislocation pile-up model of Smith [49] to model the nucleation of cracks at grain-boundary carbides. This type of model can be suitable for situations in which there are limited slip systems and in which, micro, but not macro, plastic straining occurs. Here we are interested in the situation where the precipitate particles are distributed throughout the matrix and there are a number of available slip systems.

For a particle strengthened material the initial yield strength is determined by the Orowan bowing stress (see for example [45]). As the material is deformed plastically Orowan loops are initially generated around the particles, but after one or two loops are formed, the bypass process is more readily accommodated by the punching out of vacancy and interstitial prismatic loops from the particles [45]. Using geometric arguments, Ashby [45] demonstrates that the number of prismatic loops increases in proportion to the plastic strain. These loops interact with gliding dislocations on other slip planes, leading to strain hardening of the material. This model results in quadratic hardening. Also, as the vacancy loops accumulate the tensile stress on the particle gradually builds up, with the stress due to the local dislocation structure increasing linearly with increasing plastic strain. The dominant contribution to the stress at the particle comes from the closest dislocation. If we assume that the loops spread to the mid-point between particles and the body contains a random distribution of particles we can express the stress normal to the particle due to the presence of the loops in the form:

$$\sigma = \alpha \mu_m f^{1/2} \epsilon^p \tag{1}$$

where  $\alpha$  is a dimensionless constant,  $\mu_m$  is the shear modulus of the matrix, f is the volume fraction of precipitate particles and  $\epsilon^p$  is the plastic strain. This stress arises from a short range interaction between the loops and particles and is not captured by purely continuum models of the plastic deformation process. Here we want to develop a combined continuum/cohesive zone model, that reflects as accurately as possible the processes that occur at a microstructural scale. We need to note that:

- i. The strain hardening arising from the presence of the particles is greater than predicted by a continuum composite constitutive model and this needs to be built into the hardening response of the matrix.
- ii. The stress at the matrix/carbide interface is greater than that predicted by a continuum analysis (even taking into account the additional hardening in (i) above). The continuum model gives an apparent stress normal to the interface. We need to relate this to the "actual stress" at the interface, but since the continuum model deals in terms of apparent stresses we need to express our constitutive properties in terms of these stresses.

Computa-

For the volume fraction of particles observed in practice a continuum model will produce negligible macroscopic hardening [44]. Thus the constitutive law we should employ for the matrix is that of the particle reinforced material, which we can either determine using Ashby's model [45] or from direct experimental measurements of the constitutive response. We assume that the stress at the interface is that given by the continuum analysis plus the short range stresses due to the local dislocation structure, which, as noted above is directly proportional to the plastic strain. Here we assume that the appropriate measure of strain is the Von Mises effective strain. Thus the actual stress normal to the interface  $\sigma_n^{\alpha}$  is:

$$\sigma_n^{\alpha} = \sigma_n + \alpha \mu_m f^{1/2} \epsilon^p \tag{2}$$

where  $\sigma_n$  is the normal stress given by the continuum analysis. Now consider a cohesive zone model for the interface in which:

$$\sigma_n^{\alpha} = \sigma_c f(\delta) \tag{3}$$

where  $\sigma_c$  is the cohesive strength and  $f(\delta)$  is a function of the opening displacement  $\delta$  across the interface. Substituting Eq. (3) into Eq. (2) we obtain:

$$\sigma_n = \sigma_c f(\delta) - \alpha \mu_m f^{1/2} \epsilon^p \tag{4}$$

We further assume that  $\sigma_c$  is a function of the hydrogen content, so that:

$$\sigma_c = \sigma_c^0 \Phi(c) \tag{5}$$

where  $\sigma_c^0$  is the cohesive strength in the absence of hydrogen and  $\Phi(c)$  is a function of the hydrogen concentration, c. Here we assume a simple linear relationship for  $\Phi(c)$ :

$$\Phi(c) = (\xi - 1)c + 1 \tag{6}$$

where  $\xi < 1$  is a softening parameter. Following [46] we assume a simple triangular form for  $f(\delta)$  under monotonic loading, as shown in Fig. 5a, where:

$$f(\delta) = \frac{2\delta}{\delta_f} \qquad \delta \le \frac{\delta_f}{2}$$

$$f(\delta) = 2(1 - \frac{\delta}{\delta_f}) \qquad \frac{\delta_f}{2} \le \delta \le \delta_f$$
(7)

In these expressions,  $\delta_f$  is the maximum opening at which failure of the interface occurs. If the interface experiences an opening beyond the peak of Fig. 5a, to a maximum value  $\delta_m$ , we assume that unloading and reloading occurs along a radial line to the origin, such that:

$$f(\delta) = \frac{2\delta_m}{\delta_f} \qquad \delta_m \le \frac{\delta_f}{2} f(\delta) = 2(1 - \frac{\delta_m}{\delta_f})\frac{\delta}{\delta_m} \qquad \frac{\delta_f}{2} \le \delta_m \le \delta_f$$
 (8)

Philosophical Magazine

The area under the traction-separation law in Fig. 5 represent the work of fracture of the material that decreases as the hydrogen content c increases as shown in Fig. 6 as a consequence of Eq. (2). We adopt a similar set of equations for mode II loading at the interface (Fig. 5b). The cohesive shear strength  $\tau_c$  depends on hydrogen content according to:

$$\tau_c = \tau_c^0 \Phi(c) \tag{9}$$

Computa-

where  $\tau_c$  is the cohesive shear strength in the absence of hydrogen and  $\Phi(c)$  is given by Eq. (6). The dislocation loops generated to accommodate plastic slip do not induce a shear stress at the interface. Thus the local dislocation does not modify the cohesive law in shear.

These equations have been implemented within the commercial finite element code ABAQUS [52] using the user element (UEL) facility. Under mixed mode loading we use the same interpolation scheme as described by [39].

#### 5. Carbide-Matrix interface finite element model

Experimental observations discussed in Sec. 3.1 suggest that within the featureless zone the failure surface consists of planes of intense plastic deformation, facilitated by decohesion around the particles. The model described in Sec. 4 can be embedded ahead of a crack tip and combined with models of hydrogen diffusion to evaluate the detailed crack growth process. Before doing this it is instructive to examine the fundamental problem of the response of a body which contains a regular array of  $M_7C_3$  carbide particles, whose scale is such that the hydrogen content in the matrix is uniform over the timescale of interest.

We further assume that the hydrogen content at the core of dislocations and the particle/matrix interface are in equilibrium with that in the matrix. Thus we can express the constitutive response in term of a single hydrogen concentration, which we take to be that in the matrix. Further, the plastic strain that appears in eqns (2) and (4) is the average strain over a length scale comparable with the spacing of the particles.

Fig. 7 shows a representative unit cell which contains a single carbide particle. Periodic boundary conditions are employed at the boundaries to reflect the interactions with neighbouring cells.

The model consists of three different zones:

- 1. Linear elastic elements to model the  $M_7C_3$  carbides.
- 2. Cohesive elements (user-defined) at the interface between carbide/matrix to model the decohesion processes. A cohesive element has been coded as a UEL subroutine within ABAQUS in order to model a bilinear traction-separation law as a function of hydrogen content (Fig. 6) and of amount of plastic strain. The area under the traction-displacement curve represents the energy required to form a new surface as shown in Fig. 5.  $G_{IC}$  and  $G_{IIC}$  are respectively the interfacial critical energy release rates in mode I and mode II. These can be determined directly from the cohesive laws of Eqns. 3 and 7.
- 3. Continuum elements that represent the elastic-plastic matrix behaviour. Microscopic studies [47] demostrated that the local flow stress of the material is a decreasing function of the hydrogen concentration in the environmental cell (Fig. 8). A description of the effect of the hydrogen content on the flow stress is given as

O. Barrera and A.C.F. Cocks

follows [15]:

$$\sigma_Y = \sigma_0^H (1 + \frac{\epsilon^p}{\epsilon^0})^{\frac{1}{n}} \tag{10}$$

Computa-

where  $\sigma_0^H = \Psi(c)\sigma_0$  is the initial yield strength in the presence of hydrogen that decreases with increasing hydrogen concentration.  $\Psi(c)$  is a monotonically decreasing function of hydrogen concentration.  $\epsilon^0$  is the initial yield strain in the absence of hydrogen,  $\epsilon^p$  is the plastic strain and n is the hardening exponent which is considered not to be affected by hydrogen. For simplicity, we will ignore swelling due to introduction of hydrogen into a material.

Eq. 10 has been implemented in a UMAT subroutine within ABAQUS. Eq. 10 models the effect of hydrogen induced material softening, this is to be viewed as an attempt to describe the experimental observations of the effect of hydrogen on dislocation mobility [14].

Cohesive zone elements are introduced at the interface between the matrix and carbide. The overall continuum response depends on the properties of the matrix and cohesive zone, the purpose of this paper is to explore both the decohesion (HID) and localized plasticity (HELP) mechanisms that occur at the dissimilar weld 8630/625 interface following the experimental observations discussed in Sec. 3. The model as described in Sec. 4 allows us to investigate different scenarios whereby the hydrogen content may affect only one or both of the cohesive properties of the CZM and the elasto-plastic properties of the matrix.

#### 5.1. Numerical results

The object of this paper is to investigate how the key parameters of the model that are relevant to the HELP and HID mechanisms in the 8630/625 interface welds determine the macroscopical material response. The relevant parameters are:  $\alpha$ ,  $\sigma_c^0$  (Eq. (4)),  $\sigma_0^H$ , n (Eq. (10)) and the hydrogen functions:  $\Phi(c)$  (Eq. (6)) and  $\Psi(c)$  (Eq. (10)). The detailed failure mechanisms depend on two factors: (1) the ratio between cohesive strength and yield strength of the matrix  $\sigma_c^0/\sigma_0^H$  and (2) how these properties are influenced by the hydrogen concentration (driven by the functions  $\Phi(c)$  and  $\Psi(c)$ ).

Here we concentrate on the macroscopic response of an element of material which contains a regular distribution of carbide particles. Fig. 7 shows a representative unit cell, which is subjected to displacement boundary conditions such that the macroscopic uniaxial strain is increased at a constant rate. Recent TEM studies [50] suggest that the featureless zone contains a volume fraction of  $M_7C_3$  particles of the order of 22%. Their detailed shape is currently unclear, and here we assume that they are circular in plane strain as shown in Fig. 7. In the simulations presented below we assume that E = 200 GPa,  $\nu = 0.3$ ,  $\alpha = 0.34$  in Eq. (2) and n = 10,  $\epsilon^0 = \sigma_0/E = 0.0005$  in the isotropic plasticity model of Eq. (10). Curve (a) of Fig.9 shows the response for the situation where hydrogen does not influence the material properties and the matrix is perfectly bonded to the carbide particles. We treat this as a reference against which the response for other combinations of material properties can be compared.

Hydrogen influences only cohesive properties.

Consider first the situation where hydrogen only affects the cohesive properties of the interface, i.e.  $\Psi(c) = 1$  and  $\Phi(c)$  is a monotonically decreasing function of the hydrogen content. It is instructive to consider two limiting cases. If the interface is strong and does not fail as the material is deformed, the details of the way in which

hydrogen affects the interfacial properties does not influence the macroscopic behaviour and the response is as shown in curve (a) of Fig. 9. Zahl et al. [44] examined the plane strain response of a material reinforced by a square array of circular particles. They demonstrate that for a volume fraction of particles, f, less than 0.345 the limit stress for a composite with an elastic perfectly plastic matrix is equal to the plane strain yield strength of the matrix, i.e. the presence of the particles does not change the limit state. For a strain hardening material, the stress corresponding to a given macroscopic effective strain for the composite is higher than that for the matrix alone by a factor  $\beta$ . For f = 0.23 and n = 10, they find that  $\beta \approx 1.04$ , i.e. as noted in Sec. 5 a continuum model predicts that the presence of the particles results in only a small hardening of the constitutive response. This is reflected by the fact that curve (a) of Fig. 9 is similar to the curve for c=0 in Fig. 8 (taking into account the plane strain enhancement of the yield strength). The other extreme situation shown in Fig. 9 is for the situation where the carbide is replaced by a pore (curve c). The uniaxial response of the porous material is plotted as curve (c) in Fig. 9. For a 2-D array of pores the yield surface for a given volume fraction of pores is given by [53]:

$$\bar{\sigma} = \sqrt{\frac{\sigma_e^2(1+f)}{(1-f)^2} + \frac{3\sigma_m^2}{(\ln(1/f))^2}} = \sigma_y$$
 (11)

in plane strain, where  $\sigma_e$  is the von Mises effective stress,  $\sigma_m$  is the mean stress and  $\sigma_y$  is the uniaxial yield strength. For uniaxial plane strain loading and f=0.23, this equation suggests that the presence of the pores reduces the limit stress by about a factor  $\frac{2^{rd}}{3}$  compared with that of the matrix or a particle strengthened material. Note that the level of strain considered in Fig. 9 is small. There is limited pore growth as the material is strained and net hardening of the porous material occurs. Under these conditions it can be shown that the stress strain response for the porous material has the same functional form as the matrix and particle strengthened material, with the stress at any prescribed strain reduced by a constant factor. It is evident from Fig. 9 that the scaling factor of 2/3 given by Eq. (11) applies throughout the deformation process for this volume fraction of pores.

Now consider the situation where the body contains an array of particles, but the cohesive properties of the particle/matrix interface depend on the hydrogen concentration. Curve (b) of Fig. 9 shows the resulting response for the situation where the cohesive strength in the absence of hydrogen,  $\sigma_c^0$ , is equal to 200 MPa and decreases as  $\Phi(c)$  monotonically decreases (Eq. (5)) from 1 (when c=0) to 0.1 (when c=1). The initial yield stress of the matrix  $\sigma_0^{H}$  is constant and equal to 100 MPa, with the function  $\Psi(c)$  remaining equal to 1. Throughout the process the response is bounded from above and below by the perfectly bonded and porous body results. The response initially follows that of the perfectly bonded material. As the material is deformed plastically, the stress experienced at the particle matrix interface increases due to strain hardening of the matrix and the local interaction with punched out dislocations. Simultaneously, the cohesive strength of the interface gradually decreases as the result of the increase in hydrogen concentration. Eventually, the stress at the poles reaches the cohesive strength. This occurs at a macroscopic strain of about 0.5%. Cracks form at these locations and gradually propagate towards the particle equator. In the process, the macroscopic response evolves towards that of the porous material of curve (c) in Fig. 9. Under the loading conditions employed here, the interface only

Computa-

partially debonds, with a compressive interface stress generated in the vicinity of the particle equators. Never-the-less, the macroscopic limiting behaviour is well

approximated by that for the porous material.

Fig. 9 shows the contours of accumulated effective plastic strain within the unit cell at a macroscopic nominal strain of 2.5%. For the perfectly bonded situation most of the matrix deforms plastically, while for the porous material, strain is concentrated within bands of intense shear between pores in adjacent cells. For the situation where the interface debonds as the material deforms plastically, the deformation pattern is intermediate between these two extremes, but following the initiation and growth of the interfacial cracks deformation becomes increasingly concentrated within bands that link debonded regions. Fig. 10 shows further details of the evolution of plastic strain at three instants during the loading of curve (b) in Fig. 9. At the beginning of the calculation the yield stress of the matrix is lower than the cohesive strength, hydrogen atoms in the lattice and in the traps are in equilibrium with local stress (1). By increasing the hydrogen content the barriers to dislocation motion are lowered and stress at the carbide increases (Eq. (2)). The amount of deformation increases in a localized region adjacent to the region where a partial decohesion initiates (2). Complete decohesion at the carbide/matrix interface (3) is followed by intense localized plastic deformations between microcracks.

The important feature of these plots is the net softening of the constitutive response following debonding at the particle/matrix interface. In situations where macroscopic stress gradients exist in a component, such as ahead of a crack, the strain will become localised on a length scale determined by the macroscopic boundary conditions, which will superimpose on the microscopic deformation processes examined here. The interaction of these microscopic and macroscopic deformation processes and how they influence the pseudo cleavage process described in section 3 is the subject of ongoing research.

Hydrogen influences only yield properties of the matrix.

Now consider the case in which hydrogen affects only the matrix properties i.e.  $\Phi(c)$  is constant and equal to one and  $\Psi(c)$  varies from one when the hydrogen content is c=0 to 0.1 when the hydrogen content is ramped up to c=1. The matrix yield stress of the virgin material  $\sigma_0^H$  is equal to 100MPa. During the process of ramping up the hydrogen the reference yield stress of the matrix  $\sigma_0^H$  decreases from 100MPa (when c=1) to 10MPa (when c=0). The cohesive strength  $\sigma_c^0$  is kept constant. Fig. 11 shows the macroscopic stress-strain curve together with the distribution of microscopic effective plastic strain at the max hydrogen content (c=1) for three study cases: (d)  $\sigma_c^0$ = 200MPa, no cracks form at the interface and this is equivalent to perfect bonding between matrix and carbide, (e)  $\sigma_c^0$ = 70MPa partial decohesion of the matrix/carbide interface now occurs, (f) the carbide is replaced by a hole.

In all of the cases (d), (e) and (f) as we increase the hydrogen content the matrix softens (Eq. (10)) due to the fact that by increasing the hydrogen content the barriers to dislocation motion are lowered. In situations where debonding does not occur (d) hydrogen atoms in the lattice and in the traps stay in equilibrium with local stress and the distribution of microscopic plastic strain at the max hydrogen content is reasonable uniform around the particles. The peak stress normalized with respect to  $\sigma_0^H$  is 1.3 and the corresponding value of strain is 0.5%. In the case of partial decohesion (e) the amount of deformation increases in a localized region adjacent to the region where a partial decohesion initiates (i.e. microcrack formation sites). The peak stress and peak strain are respectively 1.07 and 0.25%, which are lower than for case (d) consistent to the loss of strength due to the

partial debonding of the carbide/matrix interface. For the situation where the particle is replaced by a hole the peak stress is further reduced to 0.8 and plastic flow is localized along bands. As with the problem of Fig. 9 described above the macroscopic response in case of partial decohesion (e) is bounded between the responses of perfect bonding between carbide/matrix (d) and the hole/matrix system (f). The peak stress of curve (e) depends on the value of the cohesive strength  $\sigma_c^0$  i.e. the ratio  $\sigma_c^0/\sigma_0^H$ . Increasing this ratio increases the value of the peak stress and the strain at which the peak occurs. If the ratio  $\sigma_c^0/\sigma_0^H \approx 1$  then partial decohesion of the interface occurs. Hence, part of the original strengthening of the carbide/matrix system becomes lost and localization of plastic flow will occur leading to a combined deformation mechanism HELP+HID. If the ratio  $\sigma_c^0/\sigma_0^H < 1$  we observe complete decohesion and the macroscopic response approaches that of the hole/matrix system.

In the situation considered here, softening occurs primarily as a result of the effect of hydrogen on the mobility of the dislocations. If the interface is weak, decohesion can reduce the peak stress and the level of strain at which the peak is observed. Hydrogen influences cohesive and matrix properties.

We now consider the situation where hydrogen affects both the cohesive strength and the yield stress of the matrix  $(\Psi(c))$  and  $\Phi(c)$  vary with hydrogen concentration). We ramp up the hydrogen content from c=0 to c=1 as the macroscopic nominal uniaxial strain is increased to 2.5%. Both the cohesive strength in the absence of hydrogen  $\sigma_c^0$  (Eq. 3) and the matrix yield stress of the virgin material  $\sigma_0^H$  are set equal to 200 MPa (Eq. 10). The functions  $\Phi(c)$  and  $\Psi(c)$  monotonically decrease from 1 (when c=0) to 0.1 (when c=1). During the process of ramping up the hydrogen the reference yield stress of the matrix  $\sigma_0^H$  decreases from 200 MPa to 20 MPa. The cohesive strength  $\sigma_c$  decreases faster due to the influence of the plastic strain in the second term of Eq. 4. We observe two interacting phenomena: i) decohesion (HID) and ii) enhanced localized plasticity (HELP). Fig. 12 shows the macroscopic nominal stress - strain curve together with the distribution of microscopic effective plastic strain and the extent of the region around the particle which has decohered at three instants during the loading. For the combination of properties employed here, decohesion (HID) is initiated at the top and bottom of the carbide particle early during straining (1). As deformation proceeds and the hydrogen content increases microcracks fully develop at the particle/matrix interface (2) which open due to plastic deformation of the surrounding matrix (HELP). Plastic flow then localizes (3) along bands between microcracks formed at adjacent carbides.

The results reported here although related to a simple problem, address some important issues of the HELP and HID modelling that we presented in this paper. The evolution of plastic strain in both Fig. 10 and Fig. 12 shows that HELP and HID mechanisms act in synergy, plastic flow is localized once the interface carbide/matrix has decohered. At this scale the resulting fracture surface is characterized by planes of intense localized plastic strain between the decohesion zones at the carbide/matrix interface. The extent to which the softening processes described here influences the detailed morphology of fracture surfaces observed in practice and described in section 3 still needs to be explored and is the subject of ongoing research.

O. Barrera and A.C.F. Cocks

Magazine

Computa-

#### 6. Conclusion

A model of the failure process of a dissimilar AISI8630/IN625 weld has been proposed. The model developed here is based on a classical continuum mechanics formalism. The scale of the particles is such, however, that the interaction of the particles with discrete dislocations and the dislocation structures generated around the particles play an important role in determining the constitutive response. We have incorporated some of these effects into the model developed here by making use of classical models of the response of particle strengthened materials [42, 45] to modify both the matrix properties and the properties of the interface. In practice, decohesion at the particle matrix interface will reduce the rate of hardening in the matrix (since prismatic dislocation loops are no longer punched out from the surface). This feature of the response is not taken into account. It will have some influence on the post peak stress softening response, but will not significantly influence the location of the peak or the initial stages of the post peak softening behaviour, which are the most important features in determining macroscopic plastic localisation, for example, ahead of a crack.

The work presented in this paper is based on experimental observations of the microstructure and fracture morphology that reveal that cracks nucleate at the interface of the  $M_7C_3$  particles in the "featureless zone" under the high stresses generated ahead of a crack tip succeeded by strain localization between the particles linking these interfacial cracks with each other. The combined effect of hydrogen on the material toughness is a result of a synergistic effect of HELP and HID mechanisms: (i) with hydrogen enhancing dislocation mobility, promoting softening and strain localization; (ii) and the combined effect of increased stress on the  $M_7C_3$  carbides due to the enhanced plastic deformation and the effect of hydrogen on the interface cohesive properties promoting decohesion at the particle/matrix interface. We simulate (1) the failure process at the interface of the  $M_7C_3$  particles and the matrix by use of a cohesive modelling approach (CZM) whose  $T-\delta$  law is a function of hydrogen content and the plastic deformation of the surrounding material. We also assume (2) that the constitutive response of the material is a function of the hydrogen content. (1) and (2) have been implemented in a UEL and UMAT subroutines in ABAQUS. The model allows us to investigate different failure mechanisms depending on the effect of the local hydrogen on i) cohesive strength or on ii) elastoplastic properties of the matrix. Here we have focused on the macroscopic material response. Further studies are required to evaluate the effect of non-uniform hydrogen concentration and stress concentrating features, such as cracks on the failure process.

The results of the simulation may be summarized as follows:

- (i) When the hydrogen affects both the cohesive strength and elastoplastic properties of the matrix, the cohesive strength decreases faster than the yield stress of the matrix due to the increase of the stress generated on a particle from prismatic dislocation loops punched out from the particle. Hence a decohesion process is initiated first at the top and bottom of the carbide particle, as deformation proceeds and the hydrogen content increases microcracks fully develop at the particle/matrix interface. Plastic flow then localizes along bands between microcracks formed at adjacent carbides.
- (ii) When the hydrogen content affects only the cohesive properties and the yield strength of the matrix remains constant (and  $\sigma_c^0 > \sigma_0^H$ ), the cohesive strength decreases with the hydrogen content and the first microcrack appears when the value of  $\sigma_c^0$  is close to  $\sigma_0^H$ . The amount of deformation then increases in a localized region adjacent to the region where a partial decohesion initiates and a complete

decohesion at the carbide/matrix interface is followed by an intense localize plastic deformations between microcracks formed at adjacent carbides. (iii) If the interface is strong and is not influenced by the hydrogen content the particles prevent localization on a microscale.

#### Acknowledgements

This research is supported by the Seventh Framework Programme (European Commission), Mintweld project: reference number 229108.

#### References

- J.P. Hirth, Metallurgical Transactions A 11(1980) p. 861
- P. Sofronis and I.M. Robertson, AIP Conf. Proc. 837 (2006) p.64.
- C.D. Beachen, Matallurgical transactions 3 (1971) p. 437.
- R.A. Oriani, Annual reviews in Materials Science 8 (1978) p.327. J.C. Scully, NATO Scientific Affairs Division, Brussels, Belgium 1971.
- [6] M.R. Louthan, Journal Fail. Anal. and Prevent. 8 (2008) p.289.
- R.P. Gangloff, Comprehensive Structural Integrity, I. Milne, R.O. Ritchie and B. Karihaloo, eds, J. Petit and P. Scott, Volume Editors, Elsevier, New York, 2003, p.31.
- A. Turnbull, Corrosion science  $34\ (1993)\ p.921.$
- S.P. Lynch, Acta metall. 36(1988) p.2639.
- [10] G.M. Pressouyre, Acta Metall. 28 (1980) p.895.
- 11] G.M. Pressouyre and I.M. Bernstein, Metall. Trans. A 12 (1981) p.835.
- [12] H. K. Birnbaum and P. Sofronis, Materials Science and Engineering, A 176 (1994) p.191.
- [13] M. L. Martin, Acta Materialia 59 (2011) p.1601. [14] P. Sofronis, Y. Liang, and N. Aravas, European Journal of Mechanics A/Solids 20 (2001) p.857.
- [15] Y. Liang, and P. Sofronis, Journal of Mechanics and Physics of Solids 51 (2003) p.1509.
- J. A. Fenske, PhD thesis: University of Illinois at Urbana-Champaign 2010.
- [17] P. Novak, R. Yuan, B. P. Somerday, P. Sofronis, and R. O. Ritchie, Journal Mech. Phys. Solids 58 (2010) p.206.
- [18] P. Sofronis, I.M. Robertson and D.D. Johnson, Project report, University of Illinois at Urbana-Champaign.
- V. Olden, C. Thaulow, R. Johnsen, E. Ostby and T. Berstad, Eng. Frac. Mec 76 (2009) p.827.
- [20] M. L. Martin, I.M. Robertson and P. Sofronis, Acta Materialia 59 (2011) p.3680.
- G.I. Barenblatt, Adv. applied mech. 7 (1962) p.55.D.S. Dugdale, J Mech Phys Solids 8 (1960) p.100.
- A. Needleman, *J Appl mech* 54 (1987) p.25.
- A. Needleman, J Mech phys solid 38 (1990) p.289.
- V. Tvergaad and J.W. Hutchinson, J Mech phys solid 40 (1992) p.1377.
- V. Tvergaad and J.W. Hutchinson, Int J solids struct 31 (1994) p.823. V. Tvergaad and J.W. Hutchinson, Philos Mag A 70 (1994) p.641.
- D.S. Shih, I.M. Robertson and H.K. Birnbaum, Acta Metall. 36 (1988) p.111. T.B. Flannagan, N.B. Mason and H.K. Birnbaum, Scr.Met. 15 (1981) p.109.
- [30] S. Takano and T. Suzuki, Acta Metall. 22 (1974) p.265.
- [31] V. C. M. Beaugrand, S. L. Smith and M.F. Gittos, Proceedings of the 28th International Conference on Ocean, Offshore and Arctic Engineering OMAE2009 Honolulu, Hawaii, USA 2009.
- [32] M.F. Dodge, H.B. Dong, M. Milititsky, R.P. Barnett, V.F. Marques and M.F. Gittos, Proceedings of the 31st International Conference on Ocean, Offshore and Arctic Engineering OMAE2012 Rio de Janeiro, Brazil 2012.
- [33] H.B. Cary and S.C. Helzer, Weldability of metals in Modern Welding Technology. E. Francis Editor, Pearson Prentic Hall: Columbus, 2005, p.403.
- I. M. Robertson and H. K. Birnbaum, Acta Metall. 34 (1986) p.353.
- [35] A. R. Troiano, Trans. ASM, 52 (1960) p.54.
   [36] E. A. Steigerwald, F.W. Schaller and A. R. Troiano, Trans. Met. Soc. AIME 218 (1960) p.832.
- R. A. Oriani and P.H. Josephic, Acta Metall. 22 (1974)p.1065.
  R. A. Oriani and P.H. Josephic, Acta Metall. 25 (1977) p.979.

- A. Turon Travesa, PhD thesis: University of Girona, Spain 2006.
  J. Simo and J.W Ju, International Journal of Solid and Structures 23 (1987) p.821.
- B.W. Kim and A.H. Mayer, Composite science and technology 63 (2003) p.695.
- S.H Goods and L.M. Brown, Acta Metal. 27 (1978) p.1.
- W. M. Garrison and N.R. Moody, J. Phys. Chem. Solids 48 (1987) p.1035.
- D.B. Zahl, S. Schmauder and R.M. McMeeking, Acta Metall 42 (1994) p.2983.
- M.F. Ashby, Strengthening Methods in crystals, A. Kelly and R.B. Nicholson, eds, Elsevier, 1971, , Chap 3.
- O. Nguyen, E.A. Repetto, M. Ortiz and R.A.Radovitzky, Int. Journal of Fract. 110 (2001) p.351.
- T. Tabata and H.K. Birnbaum, Scr. Met. 17 (1983) p.947.
- [48] K. Tanaka, T. Mori and T. Nakamura, Philosophical Magazine 21 (1970) p.267.

 $\begin{array}{lll} {\rm October} & 26, & 2012 & 16{:}41 & {\rm Philosophical} \\ {\rm tional*modelling*of*hydrogen*embrittlement*in*welded*structures} \end{array}$ Magazine Computa-

REFERENCES

- [49] E. Smith, The International Journal of Fracture Mechanics 4 (1968) p.131.
  [50] H. Kitaguchi, S. Lozano-Perez, Private communications.
  [51] M. Dodge, M. Milititsky, Private communications.
  [52] ABAQUS, 6.10-1.
  [53] A.C.F. Cocks, Unpublished work.

REFERENCES

#### 8. Figure Captions

- Fig 1. Schematic summary of interface microstructure 8630/625 showing the different types of precipitates that are present [50].
- Fig 2. SEM image of fracture morphology of interface microstructure 8630/625 showing different morphologies: "Crater-like" and terraced cleavage-type [51].
- Fig 3. Schematic representation of fracture path in Fig.2.
- Fig 4. Closer inspection of Fig. 2 in the Nickel side. Ridges are seen on cleavage faces and craters appear to have a lath-like shape [51].
- Fig 5. Bilinear traction-separation law for a) mode I and b) mode II.
- Fig 6. Bilinear traction-separation law as function of hydrogen content.
- Fig 7. Unit cell representing Carbide-Matrix system consisting of three regions: matrix, carbide and interface carbide-matrix.
- Fig 8. The effect of the hydrogen content on the flow stress of the matrix.
- Fig 9. Hydrogen influences only cohesive properties. Distribution of microscopic effective plastic strain at the max hydrogen content (c=1) for (d) perfect bonding between matrix and carbide, (e) partial decohesion of the matrix/carbide interface, (f) total decohesion of the interface.
- Fig 10. Details of the evolution of plastic strain at three instants during the loading of curve (b) in Fig. ??. Hydrogen in the lattice and in the traps is in equilibrium with local stress, then partial decohesion leads to microcrack formation. Plastic flow is then localised along bands between microcracks.
- Fig 11. Hydrogen influences only yield properties of the matrix. Distribution of microscopic effective plastic strain at the max hydrogen content (c=1) for (a) perfect bonding between matrix and carbide, (b) partial decohesion of the matrix/carbide interface, (c) total decohesion of the interface.
- Fig 12. Evolution of plastic strain for different hydrogen content affecting both the cohesive strength and the yield stress of the matrix. Decohesion at the carbide/matrix interface leads to microcracks formation followed by localization of plastic flow acting as microcracks link-up.